Non-collinear Exchange Coupling in Fe/Mn/Fe(001): Insight from a Microscopic STM View

D.T. Pierce, A.D. Davies, J.A. Stroscio, D.A. Tulchinsky, J. Unguris, and R.J. Celotta
Electron Physics Group, National Institute of Standards and Technology
Gaithersburg, MD 20899-8412

Abstract

The film growth and morphology of epitaxial Mn films grown on Fe(001) single crystal whiskers measured with scanning tunneling microscopy (STM) provides insight into the mechanism of interlayer exchange coupling in Fe/Mn/Fe(001) trilayers. The proximity model of Slonczewski for exchange coupling through an antiferromagnet predicts that the coupling angle between the ferromagnetic layers will oscillate around a mean value of 90° with an amplitude that is very sensitive to the width of the thickness distribution of the spacer layer. We measure the thickness distribution with the STM and find that the coupling angle variation predicted by the proximity model is qualitatively consistent with the actual coupling angle variations in Fe/Mn/Fe(001) measured with scanning electron microscopy with polarization analysis (SEMPA). Going beyond the proximity model and allowing for a non-uniform magnetization of the thin Fe overlayer provides an improved explanation of the results. We contrast the behavior of Fe/Mn/Fe(001), where the proximity model appears applicable, to coupling through antiferromagnetic Cr in Fe/Cr/Fe(001), where it is not, and discuss possible reasons for the difference.

PACS: 75.70.-i, 68.55.Jk, 61.16.Ch Key words: Exchange coupling, magnetic multilayer, Mn film growth, Fe whisker, STM, SEMPA, RHEED

Corresponding author: D. T. Pierce, NIST (MS 8412), Gaithersburg, MD 20899-8412
Tel: (301) 975-3711; Fax: (301) 926-2746; email: daniel.pierce@nist.gov

1.Introduction

The interlayer exchange coupling of ferromagnetic films through a metallic spacer has been extensively studied over the past decade [1]. For paramagnetic and diamagnetic metal spacer layers, the magnetic coupling is well described by quantum well models where the coupling is determined by the Fermi surface properties of the spacer layer material and the reflection amplitudes for electrons scattering at the interfaces between the spacer layer and the ferromagnetic layer [2,3]. In contrast, if the spacer layer is an antiferromagnetically ordered material such as Cr or Mn, it can no longer be considered a passive medium transmitting the indirect exchange coupling as in the quantum well picture. In such cases, the exchange coupling of the antiferromagnet to the ferromagnet at the interfaces, as well as the internal exchange coupling within the antiferromagnet, must be considered. Coupling through Cr, which has been intensively investigated, for example, in Fe/Cr multilayers [4], is a somewhat special case complicated by the spin density wave nature of antiferromagnetism in Cr. A simpler antiferromagnetic spacer might be Mn, particularly if it is grown on a ferromagnet as a bcc or bct film where it has alternating planes of moments parallel and antiparallel to the magnetization of the ferromagnet.

Filipkowski et al. [5] measured the magnetic coupling of CoFe ferromagnetic layers through a Mn spacer layer and found a very large coupling between the CoFe layers with the magnetizations at 90° to each other. They found that their magnetization curves and ferromagnetic resonance (FMR) measurements were not well described by the usual bilinear-biquadratic coupling model for the coupling energy, E_c, per unit area given by

$$E_c = -\bar{J}_1\, \hat{\boldsymbol{m}}_1 \cdot \hat{\boldsymbol{m}}_2 - \bar{J}_2 (\hat{\boldsymbol{m}}_1 \cdot \hat{\boldsymbol{m}}_2)^2. \qquad (1)$$

Here the magnetization directions of the ferromagnetic layers are given by unit vectors $\hat{\mathbf{m}}_1$ and $\hat{\mathbf{m}}_2$, and the angle between them is the coupling angle, θ. J_1 and J_2 are parameters describing the bilinear and biquadratic coupling respectively. The bar is written to emphasize that observed quantities are spatially averaged values. Depending on the sign of $\bar{J}_1$, the first term drives the magnetization directions of the two ferromagnetic layers to be parallel or antiparallel. The coupling depends on $\hat{\mathbf{m}}_1 \cdot \hat{\mathbf{m}}_2$, i.e., it is bilinear in the magnetization directions. The second term, which is biquadratic in $\hat{\mathbf{m}}_1$ and $\hat{\mathbf{m}}_2$, leads to canted or non-collinear coupling, i.e. different from 0 or 180º, when $\bar{J}_2 < 0$. To find the coupling angle in the minimum energy state, in the general case, it is necessary to include not just the terms in Eq. (1) but also other terms such as the anisotropy energies of the magnetic films.

Filipkowski et al. [5] found that their magnetization and FMR data were fit much better by another phenomenological model for the coupling energy that was proposed by Slonczewski [6] specifically for coupling through an antiferromagnetic spacer layer. The model also described subsequent Brillouin scattering [7] and magnetic circular dichroism [8] measurements on CoFe/Mn/CoFe. This model, known as the proximity or torsion model (see Sec. 2) depends on the intrinsic antiferromagnetism of the spacer and strong coupling across the interface to the ferromagnet. The behavior of the antiferromagnetic spacer depends on the *proximity* of the ferromagnetic layer. The coupling energy per unit area in the proximity model is given by

$$E_c = C_+\theta^2 + C_-(|\theta| - \pi)^2 \qquad (2)$$

where $-\pi < \theta < \pi$. The coefficients C_+ and C_- reflect the contributions of regions of the spacer layer that are, respectively, an odd or even number of monolayers (ML) thick. These coefficients are proportional to the fractional areas of the two regions and the energy to twist the magnetization in the antiferromagnet as will be explained below. For a uniform thickness spacer that is an odd (even) number of ML thick, E_c is minimized for $\theta = 0°(180°)$. For a very non-uniform spacer where the regions that are an odd number of ML thick are equal in area to those that are an even number of ML thick, the coupling angle is 90°.

The coupling of Fe/Mn/Fe was studied by Yan et al. [9] in a series of measurements on a trilayer grown on a GaAs substrate with a Mn wedge-shaped spacer layer. The magnetic hysteresis curves measured with the magneto-optic Kerr effect were found to be in better agreement with curves calculated using the proximity model of Eq. (2) than with curves calculated using the bilinear-biquadratic model of Eq. (1). In particular, Eq. (2) predicts an asymptotic approach to saturation that fits the data better than Eq. (1), which predicts full saturation of the $\boldsymbol{M} - \boldsymbol{H}$ curves at finite field. Above a Mn thickness of approximately 7 ML, Yan et al. observed a coupling angle of 90º in remanence, and found that the coupling strength oscillated with a period of 2 ML. In earlier measurements of a Fe/Mn/Fe(001) whisker trilayer, Purcell et al.[10] reported a 2 ML period oscillation in the strength of the observed antiferromagnetic coupling but did not determine the coupling angle.

Recently, using scanning electron microscopy with polarization analysis (SEMPA), Tulchinsky et al. [11] investigated the coupling through Mn in a Fe/Mn(wedge)/Fe(001) trilayer where one of the Fe layers was a single crystal Fe whisker. For Mn thicknesses greater than 4 ML, the coupling between the top Fe layer and the Fe whisker substrate is such that their magnetization directions are no longer collinear. At 9 layers and above, the coupling angle oscillates with a two-layer period between $90°-\varphi$ and $90°+\varphi$. The value of φ was found to be sample dependent and to range between approximately 10 and 30°.

For narrow growth fronts, the proximity model makes predictions about variations in coupling angle. These variations depend strongly on the atomic structure of the spacer layer, i.e. its thickness fluctuations. In this paper we report scanning tunneling microscopy (STM) measurements of the growth of Mn on an Fe(001) whisker and the resultant thickness distribution of the Mn layer. With this knowledge of the thickness distribution, the specific predictions about the coupling angle made by the proximity model can be tested by comparing to the recent SEMPA results from Fe/Mn/Fe(001) where oscillations in the coupling angle were observed.

This paper is organized as follows. In Section 2, we describe the proximity model and its predictions for a range of thickness distributions of an antiferromagnetic spacer layer. In Section 3, we report the STM measurements of Mn growth on Fe and an analysis of the Mn thickness distributions. In Section 4 we compare the predictions of the coupling angle from the proximity model, using the thickness distributions measured with the STM, to the coupling angle measured by SEMPA. In Section 5, we speculate on

the origin of the differences that have been observed in the coupling through Mn as compared to coupling through Cr. We summarize our conclusions in Section 6.

2. The proximity model and its predictions

The crucial difference between Mn and a noble metal as a spacer layer is that the Mn atoms each have magnetic moments which couple to each other and across the interface to the ferromagnet. SEMPA measurements [11] of the bare Mn wedge sample on Fe(001), before the top Fe overlayer was added, showed that the Mn moments are aligned parallel or antiparallel with the Fe whisker magnetization. For films thicker than a few ML, the magnetization of the Mn surface reverses direction with each additional ML of Mn as expected for an antiferromagnet consisting of alternating planes of ferromagnetically aligned moments, in agreement with previous measurements of Mn grown on a Fe(001) film [12]. When the interfaces between the Fe and the Mn are atomically smooth, it is possible for all spins to have their preferred alignment. However, when roughness is present at the interface, it is not possible for all spins to have their preferred alignment in the antiferromagnet, in the ferromagnet, and also across the interface. Some pairs of spins will necessarily not be in their minimum energy configuration, that is, the coupling between spins will be 'frustrated'.

The proximity model assumes a strong coupling across the interface between the interface spins in the antiferromagnet and the ferromagnet [6]. It also assumes a uniform magnetization in the Fe. With these assumptions, the frustration of the spin alignment will be relieved by a rearrangement of spins in the antiferromagnet. The proximity model describes how this rearrangement happens. For this discussion, consider a trilayer where both ferromagnetic layers are of the same material so that the coupling to the antiferromagnet is either ferromagnetic or antiferromagnetic at each interface depending on the materials. Then for perfect interfaces with a spacer layer that is an odd (even) number of ML thick, the coupling angle between the magnetizations of the ferromagnetic layers will be 0º (180º). In the presence of thickness fluctuations in the spacer layer, there is a competition between the exchange coupling through regions that are an odd or even number of ML thick and the intralayer exchange in the ferromagnetic layers. The intralayer exchange in each ferromagnetic layer leads to a minimum distance or 'response length' over which the ferromagnetic layer can change its magnetization direction just as the magnetization in a bulk ferromagnet can change direction only over a distance corresponding to the width of a Bloch domain wall.

The proximity model considers how the spins in the antiferromagnet adjust to minimize the energy within a region of lateral dimensions given by the response length of the ferromagnet to achieve a coupling angle θ between the magnetization directions $\hat{\boldsymbol{m}}_1$ and $\hat{\boldsymbol{m}}_2$ of the ferromagnetic layers. Slonczewski [6] considers the increase in coupling energy E_c in the antiferromagnet when the spins S_i and S_j in layers i and j twist relative to each other with respect to their minimum energy state by an angle ϕ_{ij}. He writes $E_c = \sum_{i,j} K_{ij} S_i S_j (1 - \cos\phi_{ij})$, where K_{ij} is the effective exchange coupling between layers i and j, and is assumed to be strongest at nearest neighbor separations. The angle ϕ_{ij} between adjacent layers is also small if the antiferromagnetic spacer is not too thin.

This is shown pictorially in Fig. 1 where, for the purpose of illustration, there is a region that is 9 ML thick and a region with twice the area that is 8 ML thick. The layers

of spheres with light gray arrows at the top and bottom represent the interface layers of the ferromagnetic films with a uniform magnetization direction. The white spheres with black arrows represent the atoms on one antiferromagnetic sublattice and the dark gray spheres the other antiferromagnetic sublattice. The arrows in Fig. 1 (a) represent the direction of the magnetic moments in each layer of one sublattice and show how the layers in the antiferromagnet "wind up" when the ferromagnetic layers are coupled at an angle θ. For clarity, only the moments in the antiferromagnetic sublattice represented by the white spheres are shown in Fig. 1 (a). In this example, the energy is minimized by the moments in the even-layered region with the larger area winding up through a smaller angle $\pi - \theta$, and the moments in the other region winding up through a larger angle θ. The winding up of the moments in the antiferromagnetic layers has led to the proximity model also being known as the *torsion* model.

Slonczewski [6] notes that when K_{ij} is rather localized and there are a sufficient number of layers n, so that $\phi_{ij} \simeq \theta / n$ in one region and $\phi_{ij} \simeq (\pi - \theta)/n$ in the other region are both small, then E_c is approximately quadratic in ϕ_{ij} and hence in θ or $\pi - \theta$ making the phenomenological expression of Eq. (2) plausible. We also note that since the coupling between two layers is quadratic in ϕ_{ij}, it is proportional to $1/n^2$; thus the total coupling E_c when there are n layers is proportional to $1/n$.

The two terms contributing to the coupling energy E_c are shown individually in Fig. 1 (c). In this example, the coupling coefficient C_- of the region where the spacer is an even number of ML thick is twice as large as C_+ because its area is twice as large. Also shown is the total coupling energy, E_c, which has a minimum from Eq. (2) (ignoring contributions from anisotropy) at the coupling angle given by

$$\theta = \pi (C_- / (C_+ + C_-)), \qquad (3)$$

which in this example is $2\pi/3$ or 120°. From this example, it can be seen that the spatial distribution of thickness fluctuations, that is the relative areas corresponding to an even or odd number of ML in the spacer within a lateral region given by the magnetic response length of the ferromagnetic layers, is crucial to the determination of the coupling angle.

We turn now to the application of the proximity/torsion model of Eq. (2) to predict the coupling angle in the Fe/Mn/Fe(001) trilayer system in this investigation. Because large atomically flat regions can be found on the Fe(001) whisker substrate [13], it is possible to get a measure of the thickness distribution by measuring the Mn growth front with the STM. A typical STM image of a 750x1000 nm region of a Mn film is shown in Fig. 2 (a). Each gray level corresponds to a change in thickness by one ML. The amount of each layer visible in the image is plotted in Fig. 2 (b). It is frequently possible to represent the growth front by a Gaussian [14], as is the case here. The mean is the average height $\bar{h}$ or thickness (9.81 ML in Fig. 2), and the standard deviation (0.6 ML in Fig. 2) is equal to the root-mean-square height variation or rms roughness, $h_{rms} = \left\langle (h - \bar{h})^2 \right\rangle^{1/2}$. Because care is taken to measure h_{rms} on a flat region of the Fe whisker, the standard deviation of the growth front can be identified with the standard deviation σ of the thickness distribution of the Mn.

The standard deviation of the thickness distribution of the Mn spacer layer gives the relative contributions of regions that are an odd or even number of ML thick to the coupling. At an average thickness of an odd or even integer number of monolayers there will be a larger contribution from regions that are an odd or even number of ML thick, respectively, if σ is not too large. At the half layer average coverage in between, there will be equal contributions from the odd and even ML thick regions leading to a coupling angle of 90° independent of the size of σ. Thus, the coupling angle will vary about 90° with the extremes depending on the size of σ. Using Eq. (3) it is possible to plot the amplitude of the coupling angle variations as a function of σ as shown in Fig. 3 (a). It is striking how rapidly the amplitude of the coupling angle changes with σ. Figure 3 (b) shows how the coupling angle would vary with Mn thickness for $\sigma = 0.3$ ML. It varies from nearly 0° to nearly 180°, where for the purposes of this illustration we have assumed that the common factor in C_+ and C_- that governs other aspects of the coupling strength does not vary with thickness over the thickness range displayed. When σ increases to 0.7 ML in Fig. 3 (b), the coupling angle oscillates with a variation of $\pm 16^\circ$ about 90°.

3. Mn/Fe growth morphology

Bulk Mn exhibits complex structural variations. The cubic α phase, which has 58 atoms per unit cell, is stable up to 727 °C. A cubic β phase with 20 atoms/cell, a fcc γ phase, and a bcc δ phase are all stable only at higher temperatures [15]. Mn grows pseudomorphically on Fe(001) in a body centered tetragonal (bct) phase [10,15,16,17]. The strained epitaxial growth stabilizes a thin film phase at room temperature that is not observed in the bulk. The structure of Mn/Fe(001) thin films has been investigated using low energy electron diffraction (LEED) [15], reflection high energy electron diffraction (RHEED) [17], extended x-ray absorption fine structure (EXAFS) [17], and grazing ion-surface scattering [18]. The in-plane lattice spacing and symmetry was found from LEED observations to be the same for Mn and Fe up to about 15 ML of Mn [10]. Quantitative LEED studies found pseudomorphic growth of a bct film with an in-plane lattice constant of 0.287 nm and an out-of-plane layer spacing of 0.1614 nm for a 12-14 ML film [15]. For Mn growth at room temperature, a RHEED study found a change in RHEED intensity oscillations between 2 and 3 ML that was confirmed by EXAFS spectra indicating a structural transition in this thickness range [17]. The layer spacing for Mn films up to 2 ML was found to be slightly less than for thicker layers [15,17]. The sensitivity to details of the sample preparation was seen in grazing ion-surface scattering, which indicated interfacial alloying of up to 60% of the Mn atoms in the first layer when deposited at an Fe substrate temperature of 287° C [18].

Our STM measurements give a detailed real space picture of the Mn growth and are thus complementary to the studies mentioned above. We focus on the morphology of Mn films in the 9-11ML range where the SEMPA measurements consistently showed oscillations in the coupling angle. We describe briefly the morphology of thinner layers to give an indication of the complexity of the growth in Mn thin films. The measurements are carried out in an ultra-high vacuum system with facilities for thin-film growth and surface characterization by room temperature STM and reflection high-energy electron diffraction (RHEED), as described previously [19].

The Fe(001) whisker offers a nearly perfect single crystal substrate [20]. Both the Fe substrate and the Mn film are very susceptible to contamination. The whiskers must be carefully cleaned and excellent vacuum conditions maintained. Mn films are deposited by thermal evaporation on the Fe whisker substrate at approximately 1 ML/min. Each film was grown continuously starting with a freshly prepared substrate at a growth temperature in the range of 160 to 200 °C. The pressure during evaporation increased from the typical base pressure of 4×10^{-9} Pa to 3×10^{-8} Pa. The STM measurements were made at room temperature. RHEED intensity oscillations were monitored during film deposition and used in conjunction with STM measurements to calibrate the Mn coverage. The uncertainty in the fractional layer coverage determined by the STM was ± 0.05 ML or less. For Mn growth on Fe(001) whisker substrates in this temperature range, RHEED intensity oscillations persist out to 15-20 atomic layers before the onset of three-dimensional growth [11]. We also use the shape of the RHEED intensity oscillations as a rough indication of the quality of growth in comparing the films grown for this STM study with those of the SEMPA study.

The growth of Mn on Fe(001) exhibits a richness and complexity that is worthy of further study but is beyond the scope of this paper. An indication of this complexity is suggested by Fig. 4, which shows a 0.6 ML film in (a) and a 5.1 ML film in (b). Both images are 250 nm across and the films were grown at 160 ± 15° C [21]. The submonolayer growth in (a) is characterized by small islands with an average spacing of order 10 nm. The islands have predominantly <100> oriented edges. In contrast, the islands for growth near 5 ML tend to be rounder and larger and more widely spaced (even after accounting for the differences in the partial layer coverages). The tendency toward larger more widely spaced islands with thicker layers is also seen in Fig. 2 (a) and Fig. 5 for Mn films near 10 ML thick. In thicker films, for example in Fig. 2 (a), one also can see small regions with rectangular cross-shaped patterns. We speculate that this may be a local reconstruction and a precursor to the three dimensional growth seen in still thicker films.

Measuring the Mn island heights provides the layer spacing. However, electronic structure differences between the exposed regions of the Fe substrate and the first Mn growth layer lead to an average island height for the first Mn layer that varies with scan voltage. The first Mn layer island height is smallest (~0.14 nm) at sample voltages near +0.2 V and increases for voltages on either side of this value, reaching at most ~ 0.16 nm. A surface state is present on Fe(001) approximately 0.2 eV above the Fermi energy [22], and appreciable tunneling into this state near sample voltages of +0.2 V will lead to an apparent decrease in the first Mn layer island height consistent with the observed trend. Although we do not have direct evidence either for or against alloying in this system, the observed variation of step height with bias of submonolayer islands suggests that Mn does not significantly alloy with the Fe substrate at this growth temperature. Alloying in this system is predicted by theory [23] and has been reported for growth near 300° C [18].

For thicker films, starting with the third growth layer, the island heights are independent of scan voltage and are the same for all thicknesses within experimental uncertainty. The average height is 0.161 ± 0.003 nm corresponding to a lattice constant in the growth direction of 0.322 ± 0.006 nm, which is consistent with the bct structure reported in the literature [10,15]. In comparison, the Fe(001) layer spacing is 0.143 nm.

This is sufficiently different from the Mn layer spacing that a single layer step in the Fe substrate, such as seen in the upper right of Fig. 4 (a), can be detected even through Mn films 10 ML thick. This is important because it allows us to avoid inadvertently including the contribution of an Fe step in the determination of the Mn thickness distribution.

The growth front of Mn on Fe(001) near 10 ML thickness is illustrated by the STM images in Fig. 5 (a-c) for Mn films grown at Fe substrate temperatures of 165 °C, 175 °C, and 200 °C, respectively. The areas of each exposed layer in these 750x500 nm images were measured as for Fig. 2. A Gaussian was fit to the data points to determine the average thickness and the rms roughness. The film thicknesses determined from the fits are 10.27 ± 0.05 ML, 9.81 ± 0.004 ML, and 10.40 ± 0.008 ML [24] for the films displayed in Fig. 5 (a-c). As discussed above, by selecting a region of the whisker without steps, the rms roughness corresponds to the standard deviation σ of the thickness distribution. The σ's are 0.61 ± 0.05 ML, 0.604 ± 0.003 ML, and 0.48 ± 0.02 ML respectively for the films grown at 165 °C, 175 °C, and 200 °C.

The RHEED intensity oscillations monitored during the deposition of each film are shown adjacent to the images. The RHEED intensity oscillations are used mainly to count the number of layers and assess the nature of the growth. The fractional layer thickness determination is obtained from the STM image. In addition to the intensity variation at layer completion, the oscillations may have a phase that depends on the glancing angle of incidence of the electron beam [25]. The RHEED oscillations are remarkably similar for the three depositions. This is consistent with the finding from the earlier SEMPA studies [11] that over this limited temperature range, the largest variations in the behavior of the RHEED intensity oscillations were from whisker to whisker indicating a sensitivity to the details of substrate quality. The same Fe whisker substrate, cleaned between depositions, was used for the STM measurements of Fig. 5. The observed lower intensity of the first oscillation peak compared to the second is likely due to the difference between the heteroepitaxial growth of the first layer and then homoepitaxial growth of subsequent layers.

4. Discussion of STM and SEMPA Results

The proximity model makes specific predictions about the amplitude of the oscillation in coupling angle for a given distribution of thickness fluctuations. We compare these predictions to actual measurements of the variation in coupling angle from SEMPA images. The SEMPA measurements were made on as-grown samples with no applied magnetic field. The direction of the Mn wedge is along the long axis of the whisker, which is also an easy magnetization axis. The SEMPA measurements were on Fe/Mn(wedge)/Fe(001) trilayers where we do not have direct STM information on the morphology of the Mn film. Therefore, to make the comparison as meaningful as possible, for the STM measurements we evaporated Mn films at deposition rates and substrate temperatures similar to those used in the fabrication of the SEMPA samples. In addition, similar Fe whiskers grown at NIST were used as substrates in both studies. A qualitative comparison of the Mn growth morphology is obtained through a comparison of the RHEED intensity oscillations. Before evaporating the Fe overlayer in the Fe/Mn/Fe trilalyer samples measured by SEMPA, the SEM beam was scanned at grazing incidence along the Mn wedge to measure the spatial RHEED intensity oscillations. For

wedge-shaped films, the spatial and temporal RHEED intensity oscillations have been shown to be very nearly the same [26].

The RHEED intensity oscillation curves of Figs. 5 and 6 exhibit fairly pronounced oscillations that indicate a nearly layer-by-layer growth. Note that unlike the RHEED curves of Fig. 5 where the measurement was halted at a given film thickness, the RHEED curves of Fig. 6 from the Mn wedges fabricated for the SEMPA investigation extend to thicknesses where the growth roughens and the RHEED intensity oscillations vanish. Comparing the RHEED curves in Fig. 5 and 6, we can say that the growth is qualitatively similar in the sense that pronounced oscillations are observed which decay over a similar thickness range. A large factor affecting the quality of Mn film growth and the resultant RHEED curve, as noted above, is the variation between Fe whisker substrates. The results in Fig. 6 (a) and (c) were from the same Fe whisker, which was different from both the whisker used for Fig. 6 (b) and a third whisker used for Fig 5.

We can make some general observations about the variation in coupling angle, calculated from SEMPA images, as a function of Mn thickness. Representative SEMPA determinations of the coupling angle variation and the corresponding RHEED intensity oscillations measured for Mn wedges grown at 150 ± 5 °C, 175 ± 6 °C and 200 ± 7 °C are shown in Fig. 6. Two curves are shown in Fig. 6 (b) for Fe overlayer thicknesses of 8 ± 0.1 ML and 20 ± 0.1 ML respectively. The Fe overlayer thickness in Fig. 6 (a) and (c) is 10 ± 2 ML. For three or fewer Mn layers, collinear ferromagnetic ($\theta = 0^{\circ}$) coupling dominates. One might speculate that this is due to a breakdown of the proximity model because the constraint that the twist angle, $\phi_{ij} \simeq \theta / n$, between adjacent layers relative to their antiparallel minimum energy state, is small no longer holds. However, we note that similar behavior has been observed for coupling through Ag [27] and Au [28], where the proximity model does not apply. At four layers and above, the coupling is no longer collinear, and above eight or nine layers the coupling oscillates about a coupling angle of 90°. Above some thickness that depends on the particular Mn deposition, the film abruptly roughens and the RHEED intensity oscillations diminish and then disappear. The oscillations in coupling angle disappear in this thickness range as well. Two other interesting trends are observed. The amplitude of the oscillation in coupling angle tends to increase with Mn thickness. The amplitude is also larger when the thickness of the Fe overlayer is larger as seen in Fig. 6 (b).

We turn to a comparison of the measured oscillations in the coupling angle in Fig. 6 and the predictions of the proximity model for the thickness distributions measured in Fig. 5. Taking half the difference of the measured coupling angles at Mn thicknesses of 10 and 11 ML as a measure of the amplitude of the coupling angle, we find amplitudes of 7°, 12°, 23° and 10° for growth at 150°C, 175°C (with 8 ML Fe), 175°C (with 20 ML Fe), and 200 °C, respectively. Within the proximity model, coupling angle amplitudes of 7°, 12°, 23° and 10° would be caused by thickness distributions with standard deviations of 0.81 ML, 0.74 ML, 0.64 ML, and 0.77 ML respectively. In comparison, standard deviations of the thickness distribution of 0.61 ML, 0.60 ML, and 0.48 ML were measured in the STM experiments for Mn growth at 165 °C, 175 °C, and 200 °C, which in the proximity model would predict amplitudes of the coupling oscillations of 28°, 30°, and 56°, respectively.

We can now reach some conclusions about the coupling in spite of the differences between the measured amplitude of the coupling angle oscillations and the predictions based on the proximity model. The measured coupling angle does not oscillate between nearly 0 and 180° as would be the case for a very narrow thickness distribution nor is the coupling angle fixed at 90° as expected for a wide thickness distribution. Rather the amplitudes of the coupling angle oscillations are in that range (see Fig. 3 (a)) where they are extremely sensitive to the width of the thickness distribution. The differences between measured coupling amplitudes and those predicted in the proximity model are accounted for by differences in the standard deviations of the thickness distributions of only a couple of tenths of a monolayer. In this sense, the measured variations in coupling angle and those predicted within the proximity model from the measured thickness distributions are in qualitative agreement. To test the proximity model quantitatively, it would be necessary to measure the thickness distribution of the Mn wedge with an *in situ* STM in the SEMPA apparatus.

The cause of the discrepancy between the predictions and the measurements of the amplitude of the coupling angle oscillations is likely due in part to differences in growth at different times on different whiskers. For higher temperature growth, possible interdiffusion at the interface could also affect the coupling. For growth at 200 °C, the difference between the SEMPA measurement and the prediction from the STM data is particularly large, a measured amplitude of 10° compared to a predicted amplitude of 56°. We note that we also observed an amplitude of only 8° (not shown) for the growth of a Mn wedge at 250 °C where strong RHEED intensity oscillations were observed.

The increase in the amplitude of the coupling angle variation with Mn thickness that is evident in Fig. 6 is surprising because it is the opposite of what is expected from the proximity model and typical growth behavior, where the width of the thickness distribution increases as a power of the thickness [14,29]. Thus, an increasing σ with increasing Mn thickness would, within the proximity model, lead to a decrease of the coupling angle variations. This strongly suggests that other mechanisms beyond the proximity model must be considered to understand the data.

We discuss limitations on the range of validity of the proximity model for its underlying assumptions to hold and how inclusion of other effects beyond this basic model can improve the explanation of the data. Slonczewski [6] considers the effect of the lateral length scale L of the spacer layer thickness fluctuations. Here, L corresponds to the island size in the STM images. He assumes that L is large compared to the spacer layer thickness as it is in our experiments. For the ferromagnetic layer to be uniformly magnetized, L must be small enough so that the intralayer exchange of the ferromagnetic layer, characterized by the exchange stiffness A, maintains the spatial uniformity of the magnetization. In Eq. (4), Slonczewski provides an estimate on the maximum size of L for the assumption of uniform magnetization to be valid [6]:

$$\{(C_+ + C_-)L \sum_{i=1,2} A_i \coth(\pi D_i / L)\} \ll 1, \qquad (4)$$

where D_i is the thickness of the respective magnetic layer. In our experiments, we do not measure C_+ and C_-. These quantities were measured, however, by Yan et al. [9] in their investigation of Fe/Mn/Fe(001) wedge shaped trilayers grown on Ag-buffered GaAs substrates. To obtain an estimate of the limits on L, we use their measurement for

C_+ and C_- of 0.118 mJ/m^2 for coupling through an approximately 10 ML thick Mn film recognizing that the meaningfulness of our estimate depends on how sensitive the strength of C_+ and C_- are to differences in the growth of Yan et al. and this work. When the thickness D_i of the ferromagnetic layers is at least as large as L, Eq. (4) gives $L \ll 42$ nm.

In our experiments, however, the whisker thickness is large (few tenths of a mm) but the Fe overlayer is thin compared to the island size. The left hand side of Eq. (4) increases rapidly when D of one of the ferromagnetic layers is much smaller than L. We estimate how well Eq. (4) is satisfied for typical conditions of our experiments, where the Fe overlayer thickness is 20 ML and L ranges from approximately 20 nm to 100 nm. For L of 20 nm and 100 nm, respectively, the left hand side of Eq. (4) is 0.8 and 14. When Eq. (4) is not satisfied, we might expect that some of the magnetic strain due to the coupling is taken up by inhomogeneities in the magnetization of the Fe overlayer in the form of ripple.

We speculate that non-uniform magnetization in a ferromagnetic layer could cause the observed increase of the amplitude of the coupling oscillations with both increasing thickness of the Mn spacer layer and the Fe overlayer. The *thickness fluctuation* model of biquadratic coupling, which predicts a non-uniform magnetization in the ferromagnetic layer, was proposed by Slonczewski to explain 90° coupling through spacer layers with a) thickness fluctuations and b) short period oscillatory exchange coupling [6, 30]. This nomenclature is somewhat confusing since thickness fluctuations are obviously also important in the proximity model. The thickness fluctuation model applies for non-collinear coupling through noble metals and can explain the non-collinear coupling observed in Fe/Cr/Fe(001) whisker trilayers as discussed elsewhere[4]. Whereas the proximity model assumes uniform magnetization in the ferromagnetic layers and describes how the regions of different thickness in the antiferromagnetic spacer wind up, see Fig. 1, to minimize the spin frustration, the thickness fluctuation model describes how an inhomogeneous state of magnetization, in the form of static magnetization waves or ripple, is established in the non-collinearly coupled ferromagnetic layers to lower the total energy [30].

The thickness fluctuation mechanism is not expected to be dominant for a spacer with strong intrinsic antiferromagnetism like Mn, but it may still make a contribution. Consider the situation where the ferromagnets couple antiferromagnetically for a spacer thickness with an even number of layers and ferromagnetically when the thickness changes by one layer on the neighboring terrace. If the regions of odd and even layer thickness within the magnetic response length of the ferromagnet are nearly equal, the tendency toward 0 or 180° coupling will be small and the energy will be minimized when the coupling angle between the ferromagnetic layers is near 90°. In this case, the second term in Eq. (1) is dominant. When the overlayer thickness t_{Fe} is small compared to the characteristic length scale L of the terraces producing the thickness fluctuations, the leading contribution to the biquadratic term in this model is [30]

$$\bar{J}_2 \propto -(\Delta J)^2 L^2 / A\, t_{Fe} \qquad (5)$$

where, as in Eq. (4), A is the exchange stiffness that characterizes the intralayer exchange coupling which hinders magnetization reversals. The quantity ΔJ is half the difference between the coupling energy for coupling at 0 and 180°. Equation (5) was derived in a

model where the coupling energy depends sinusoidally on the coupling angle, not quadratically as in the case of Mn in the proximity model. For coupling angles near 90°, Eq. (5) qualitatively describes this case as well. The prefactor will be different than in the usual thickness fluctuation model.

With this background on the thickness fluctuation model, we can see how the contribution from this additional mechanism could affect the coupling angle around 90° in Fe/Mn/Fe(001). The observed behavior of the coupling is as if there is a reduction in a mechanism that drives the coupling toward 90° with increasing Mn or Fe thickness. In the thickness fluctuation model, the size of the mechanism that drives the coupling angle toward 90° is characterized by $\bar{J}_2$, which from Eq. (5) is inversely proportional to the Fe overlayer thickness. Thus, when the thickness of the Fe overlayer is increased, the additional mechanism pushing the coupling toward 90° decreases. This might explain the increase in coupling angle with increasing Fe overlayer thickness seen in Fig. 6 (b).

A possible explanation for the variation in coupling angle with Mn thickness is as follows. The dominant factor determining the amplitude of the coupling oscillations is the coupling energy E_c in the proximity model, which decreases with the number *n* of Mn layers as $1/n$. The contribution from this additional mechanism, that is from $\bar{J}_2$, depends on $(\Delta J)^2$. Since for Fe/Mn/Fe, $\Delta J \propto C_+ + C_-$, which like E_c varies as $1/n$, the fluctuation mechanism driving the coupling angle toward 90° falls off more rapidly $(\propto 1/n^2)$ with thickness than the coupling energy $(\propto 1/n)$ in the proximity model. As this additional mechanism driving the coupling angle toward 90° decreases with increasing Mn thickness, the coupling angle increases.

5. Comparison of coupling through Mn and Cr

The interlayer exchange coupling in Fe/Cr/Fe(001) whisker trilayers, which has been intensively investigated, is quite different from the observations reported here for Fe/Mn/Fe(001) trilayers. Figure 7 shows the variation in the coupling angle for Fe/Cr/Fe as a function of the Cr layer thickness out to 50 layers. RHEED intensity oscillations are shown over the same range. Above a Cr thickness of 4 layers, the coupling angle oscillates with a period of 2 layers. There is an increase in the amplitude of the coupling angle oscillations up to about 20 layers and then the oscillation is between 0 and 180°. This striking behavior persists out to Cr thicknesses where the RHEED intensity oscillations have substantially decreased. For other samples, coupling angle oscillations of this type persist to a Cr thickness of 75 layers where the RHEED intensity oscillations have decreased to nearly zero [4, 31]. Unfortunately, we do not have STM images of the thickness fluctuations for these high coverages. However, comparing to the Mn RHEED data of Fig. 5, the relative decrease in the intensity of RHEED oscillations would suggest that there are also significant thickness fluctuations in the Cr. Hence the coupling angle oscillations from 0 to 180° in Fe/Cr/Fe cannot be explained by the proximity model, which would predict oscillations closer to 90°. Instead, we believe the Cr data can be explained by Eq. (1). The J_1 for the short period oscillation is caused by the spin density wave (SDW) antiferromagnetism of the Cr, and the long period oscillation can be explained in the quantum well picture [4,32]. The biquadratic coupling that is observed when the bilinear coupling is small, including the variation in the strength of J_2 as a function of Cr thickness, can be explained by the thickness fluctuation model. We note

that unlike the situation for exchange coupling in Fe/Cr/Fe(001) whiskers, Schreyer et al. [33] have reported neutron scattering evidence for helical ordering of Cr moments in Fe/Cr superlattices, a behavior that has been attributed to the higher density of steps in the superlattices [34].

While the two pictures of interlayer exchange coupling represented by Eqs. (1) and (2) are oversimplified phenomenological models, it is nevertheless of interest to inquire into the differences between Cr and Mn which allow Cr to be described by Eq. (1) but require the proximity model of Eq. (2) to explain the coupling through Mn. Both Cr and Mn grown on Fe(001) consist of alternating planes of ferromagnetically aligned moments. Regarding the Néel temperature T_N, the Fe substrate strongly influences T_N, and T_N has not been determined for Cr and Mn thin films grown on Fe whiskers. Regarding the magnetic moment, the peak in the spin polarized electron energy loss spectrum for Mn grown on an Fe film is at 2.9 eV [12] compared to 1.9 eV for Cr [35], indicating a larger exchange splitting in Mn and hence a larger magnetic moment than for Cr. Cr is an itinerant antiferromagnet with a spin density wave such that ordered magnetic moments at each lattice site can vary in magnitude. The proximity model assumes a short range Heisenberg exchange between local moments of fixed magnitude and is less applicable to an incommensurate spin density wave antiferromagnet like Cr, where there are long-range interactions and the moments can vary in magnitude. The proximity model seems to apply well to Mn where the moments do not vary and the interaction is thought to be more localized. Thus for Mn, the spin frustration is relieved at lowest energy cost by twisting up the moments as shown in Fig. 1. In Cr, on the other hand, the spin frustration is relieved by introducing a magnetic defect and interrupting the regular antiferromagnetic stacking of the layers. This also results in the formation of a domain wall in the Cr normal to the plane of the Cr film in the region where the Cr spins are frustrated. The energy cost of the magnetic defect is kept low by a reduction of the Cr magnetic moments near the magnetic defect. Recent tight-binding calculations by Cornea and Stoeffler support this picture [36].

6. Conclusions

The proximity or torsion model proposed by Slonczewski [6] for interlayer exchange coupling through an antiferromagnetic spacer layer predicts that the coupling angle between the magnetization directions of the ferromagnetic layers should oscillate about 90° when the standard deviation σ of the thickness distribution of the spacer layer is not too large. The amplitude of the coupling angle oscillations is very sensitive to σ in the range σ=0.3 ML to 0.7 ML. Scanning tunneling microscopy was used to investigate the growth of Mn on Fe(001). The spacing between Mn layers was determined to be 0.161 ± 0.003 nm. Although interesting complexity was seen in the morphology of Mn thin films, we focused on measuring the rms roughness of Mn films approximately 10 ML thick. Because the Fe whisker substrate is very flat, the roughness measurement gives the standard deviation σ of the thickness distribution of the Mn film. We compared coupling angle variation predicted within the proximity model for the σ measured with the STM to the actual coupling angle in Fe/Mn/Fe(001) whisker trilayers measured by SEMPA. RHEED intensity oscillation measurements of both the STM and SEMPA samples indicated similar growth. We conclude that the measured coupling angle variation is generally consistent in a qualitative way with the predictions of the proximity model. We speculate that the observed increase in coupling angle with increasing Mn

thickness and Fe overlayer thickness could be due to non-uniform magnetization in the thin ferromagnetic layer as described by the thickness fluctuation model. There is a substantial difference in the variation in the coupling angle of an Fe film to an Fe(001) whisker through a Cr spacer and a Mn spacer. We suggest that the failure of the proximity model to describe the variation of the coupling angle for Cr is due to the spin density wave nature of the antiferromagnetism in Cr and the associated longer-range interactions and variability of the magnetic moments.

Acknowledgements

We thank John Slonczewski for reading the manuscript and for helpful discussions concerning his models. We are especially grateful to Mark Stiles for very helpful discussions throughout this work. This work was supported in part by the Office of Naval Research.

Figure Captions

Figure 1. The proximity model. a) The gray arrows give the directions of magnetization, $\hat{\mathbf{m}}_1$ and $\hat{\mathbf{m}}_2$, of the ferromagnetic layers. The black arrows, giving the directions of the magnetic moments in the layers of one of the antiferromagnetic sublattices, show how the antiferromagnet "winds up" to minimize spin frustration. b) A region of the sample with a 9 ML thick antiferromagnetic spacer layer is shown at the left and a region with twice the area with a 8 ML spacer is shown at the right. The antiferromagnetic sublattice shown by the white spheres with black arrows is represented by the black arrows in (a). The magnetic moments in the larger region wind up through the smaller angle $\pi - \theta$. c) The coupling energy E_c is plotted with the two terms contributing to it. The coupling coefficient for an even number of ML, C_-, is taken as twice as large as C_+ in keeping with the schematic in (b).

Figure 2. a) An STM image of a 750 x1000 nm region of a 9.81 ML Mn film where changes in gray levels correspond to single atom height differences. b) The fraction of each layer exposed in (a) is measured and plotted for each layer. The growth front is fit well by a Gaussian.

Figure 3. a) The amplitude of the coupling angle variations predicted by the proximity model for a given σ of the thickness distribution is shown for regions of the antiferromagnetic spacer that are an odd (even) number of ML thick by the solid (dashed) line. b) The predicted variation in the coupling angle as the thickness varies is shown for spacer layer thickness distributions with σ=0.3 ML and σ=0.7 ML.

Figure 4. STM images 250 nm across from a) an 0.6 ML Mn film and b) a 5.1 ML film. The island shapes and sizes are very different even though both films were grown at 160 °C. The edges of the image are near <100> directions. A one atom high step in the Fe whisker is visible in the upper right of (a).

Figure 5. STM images 750 x 500 nm for films grown at 165 °C, 175 °C, and 200 °C and the corresponding RHEED intensity oscillations measured during growth are shown in (a-c) respectively. In the STM images (a-c) respectively the film thickness is 10.27 ML, 9.81 ML, and 10.40 ML ML, and the standard deviation of the thickness distribution σ is 0.61 ML, 0.60 ML, and 0.48 ML.

Figure 6. SEMPA determination of the variation in coupling angle in Fe/Mn(wedge)/Fe(001) is shown in (a-c) for Mn wedges grown at 150 °C, 175 °C and 200 °C respectively, along with the corresponding spatial RHEED intensity oscillation measurements from the completed Mn wedges. Two curves are shown in (b) for Fe overlayers of 8 ML and 20 ML.

Figure 7. a) The coupling angle variation measured by SEMPA for an Fe/Cr(wedge)/Fe(001) trilayer. b) The corresponding RHEED intensity oscillations from the Cr wedge.

References

1 M. D. Stiles, J. Magn. Magn. Mater. **200**, 322 (1999), and references therein.
2 P. Bruno, J. Magn. Magn. Mater. **121**, 248, (1993); Phys. Rev. B **52**, 411 (1995).
3 M. D. Stiles, Phys. Rev. B **48**, 7238 (1993).
4 D. T. Pierce, J. Unguris, R. J. Celotta, and M. D. Stiles, J. Magn. Magn. Mater. **200**, 290 (1999).
5 M. E. Filipkowski, J. J. Krebs, G. A. Prinz, and C. J. Gutierrez, Phys. Rev. Lett. **75**, 1847 (1995).
6 J. C. Slonczewski, J. Magn. Magn. Mater. **150**, 13 (1995).
7 M. Chirita, G. Robins, R. L. Stamps, R. Sooryakumar, M. E. Filipkowski, C. J. Gutierrez, and G. A. Prinz, Phys. Rev. B **58**, 869 (1998).
8 V. Chakarian, Y. U. Idzerda, H. J. Lin, C. Gutierrez, G. A. Prinz, G. Meigs, and C. T. Chen, Phys. Rev. B **53**, 11313 (1996).
9 S. S. Yan, R. Schreiber, F. Voges, C. Osthöver, and P. Grünberg, Phys. Rev. B **59**, R11641 (1999); S. S. Yan, P. Grünberg, and L. M. Mei, J. Appl. Phys. **88**, 983 (2000).
10 S. T. Purcell, M. T. Johnson, N. W. E. McGee, R. Coehoorn, and W. Hoving, Phys. Rev. B **45**, 13064 (1992).
11 D. A. Tulchinsky, J. Unguris, and R. J. Celotta, J. Magn. Magn. Mater. **212**, 91 (2000).
12 T. G. Walker and H. Hopster, Phys. Rev. B **48**, 3563 (1993).
13 J. A. Stroscio and D. T. Pierce, J. Vac. Sci. Technol. B **12**, 1783 (1994).
14 D. T. Pierce, J. A. Stroscio, J. Unguris, and R. J. Celotta, Phys. Rev. B **49**, 14564 (1994).
15 S. K. Kim, Y. Tian, M. Montesano, F. Jona, and P. M. Marcus, Phys. Rev. B **54**, 5081 (1996).
16 B. Heinrich, A. S. Arrott, C. Liu, and S. T. Purcell, J. Vac. Sci. Technol. A **5**, 1935 (1987).
17 S. Andrieu, M. Finazzi, P. Bauer, H. Fischer, P. Lefevre, A. Traverse, K. Hricovini, G. Krill, and M. Piecuch, Phys. Rev. B **57**, 1985 (1998).

18 T. Igel, R. Pfandzelter, and H. Winter,Surf. Sci. **405**, 182 (1998).
19 J. A. Stroscio, D. T. Pierce, and R. A. Dragoset, Phys. Rev. Lett. **70**, 3615 (1993).
20 A. S. Arrott, B. Heinrich, and S. T. Purcell, in: Kinetics of Ordering and Growth at Surfaces, ed. M. G. Lagally (Plenum, New York, 1990) p. 321.
21 The infrared pyrometer measurements of the sample temperatures in the STM reported here all have an uncertainty of $\pm 15^{\circ}$ C.
22 J. A. Stroscio, D. T. Pierce, A. Davies, R. J. Celotta, and M. Weinert, Phys. Rev. Lett. **75**, 2960 (1995).
23 B. Nonas, K. Wildberger, R. Zeller, and P. H. Dederichs, Phys. Rev. Lett. **80**, 4574 (1998).
24 The quoted uncertainties in the film thickness and standard deviation of the thickness distribution represent one standard deviation as determined from the fit of a Gaussian to the measured fractional areas exposed and their uncertainty for a given image.
25 Z. Mitura, S. L. Dudarev, and M. J. Whelan, J. Cryst. Growth **198/199**, 905 (1999).
26 D. T. Pierce, J. Unguris, and R. J. Celotta, in Ultrathin Magnetic Structures II, B. Heinrich and J. A. C. Bland (Eds.), Springer, Heidelberg, 1994, p. 117.
27 J. Unguris, R. J. Celotta, and D. T. Pierce, J. Magn. Magn. Mater. **127**, 205 (1993).
28 J. Unguris, R. J. Celotta, and D. T. Pierce, J. Appl. Phys. **75**, 6437 (1994).
29 Y. L. He, H. N. Yang, T. M. Lu, and G. C. Wang, Phys. Rev. Lett. **69**, 3770 (19992).
30 J. C. Slonczewski, Phys. Rev. Lett. **67**, 3172 (1991).
31 J. Unguris, R. J. Celotta, and D. T. Pierce, Phys. Rev. Lett. **69**, 1125 (1992).
32 D. T. Pierce, J. Unguris, R. J. Celotta, and M. D. Stiles, in Physics of Low Dimensions, J. Moran-Lopez (ed.), Plenum, 2000 (in press).
33 A. Schreyer, C. F. Majkrzak, T. Zeidler, T. Schmitte, P. Bödeker, K. Theis-Bröhl, A. Abromeit, J. A. Dura, and T. Watanabe, Phys. Rev. Lett. **79**, 4914 (1997).
34 R. S. Fishman, Phys. Rev. Lett. **81**, 4979 (1998).
35 T. G. Walker, A. W. Pang, H. Hopster, and S. F. Alvarado, Phys. Rev. Lett. **69**, 1121 (1992).
36 C. Cornea and D. Stoeffler, Europhys. Lett. **49**, 217 (2000).

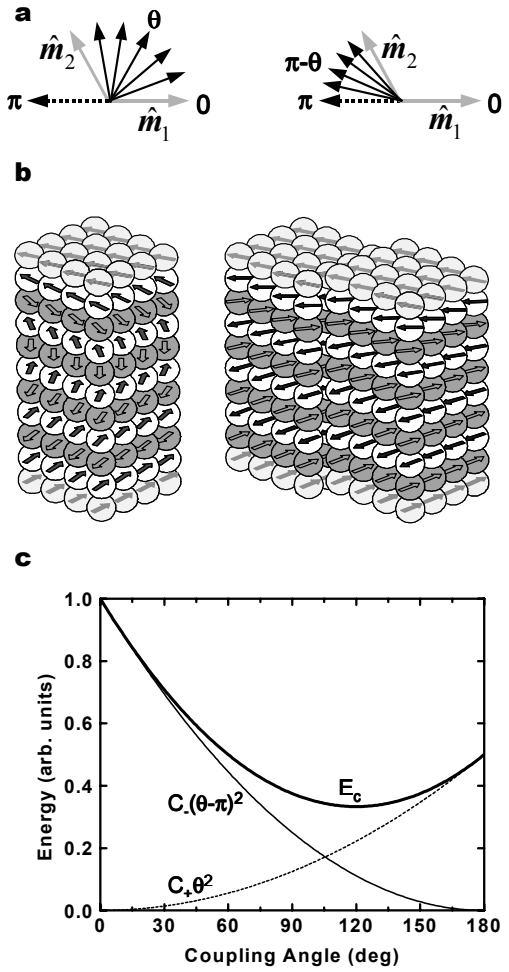
a
θ
$\hat{m}_2$
π
0
$\hat{m}_1$
π-θ
$\hat{m}_2$
π
0
$\hat{m}_1$
b
c
1.0
0.8
0.6
0.4
0.2
0.0
Energy (arb. units)
E_c
$C_-(\theta-\pi)^2$
$C_+\theta^2$
0
30
60
90
120
150
180
Coupling Angle (deg)

Fig. 1

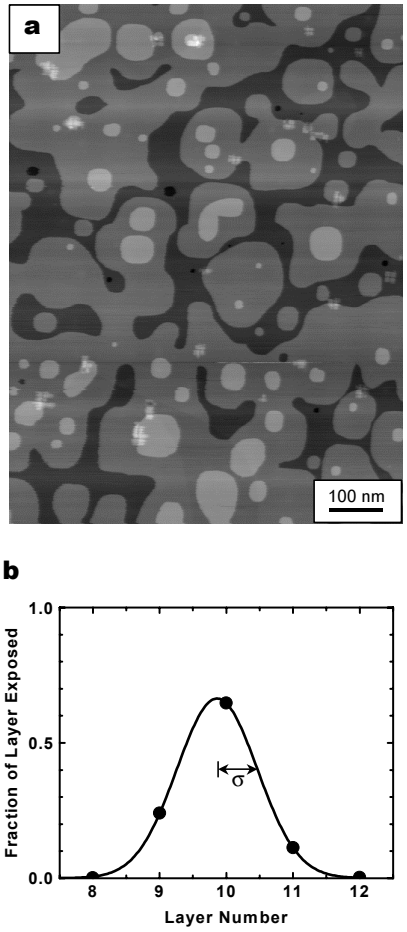
a
100 nm
b
1.0
0.5
0.0
Fraction of Layer Exposed
8
9
10
11
12
Layer Number
σ

Fig. 2

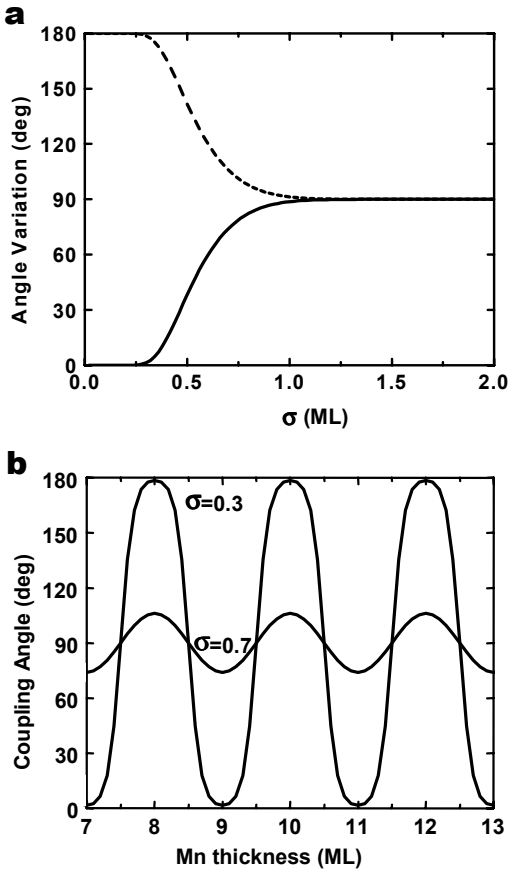
a
180
150
120
90
60
30
0
Angle Variation (deg)
0.0
0.5
1.0
1.5
2.0
σ (ML)
b
180
150
120
90
60
30
0
Coupling Angle (deg)
σ=0.3
σ=0.7
7
8
9
10
11
12
13
Mn thickness (ML)

Fig. 3

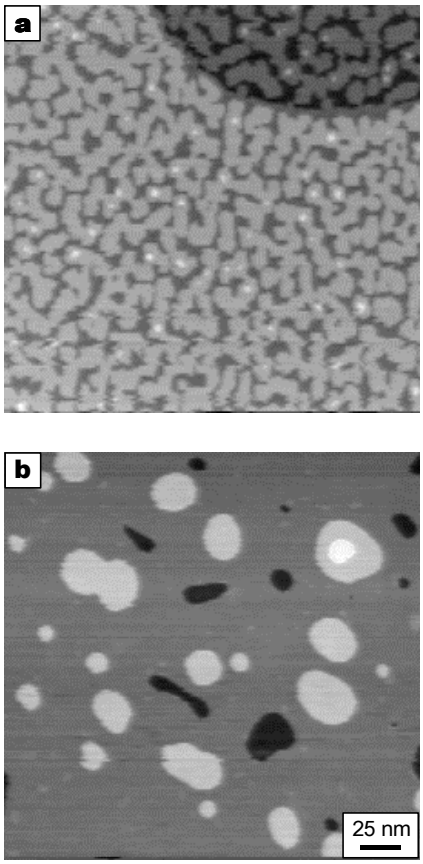

Fig. 4

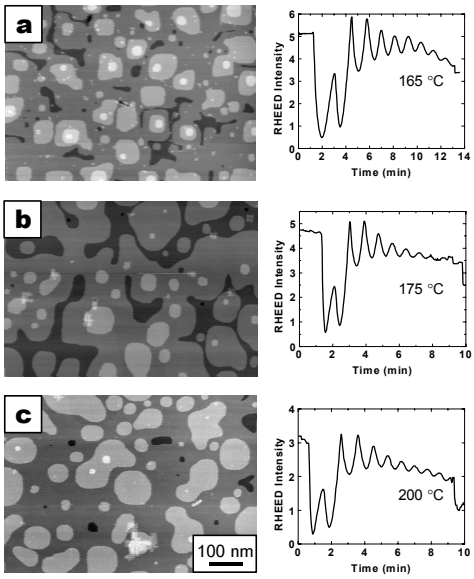

Fig. 5

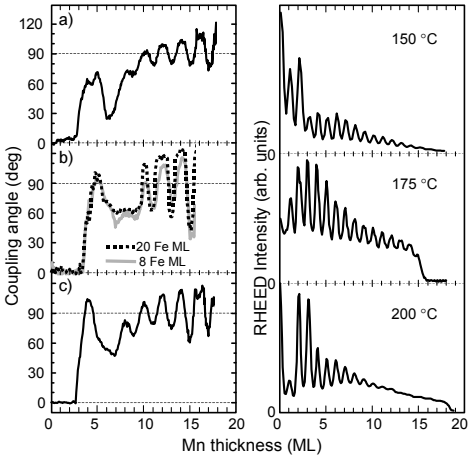
a)
b)
c)
20 Fe ML
8 Fe ML
Coupling angle (deg)
Mn thickness (ML)
150 °C
175 °C
200 °C
RHEED Intensity (arb. units)

Fig. 6

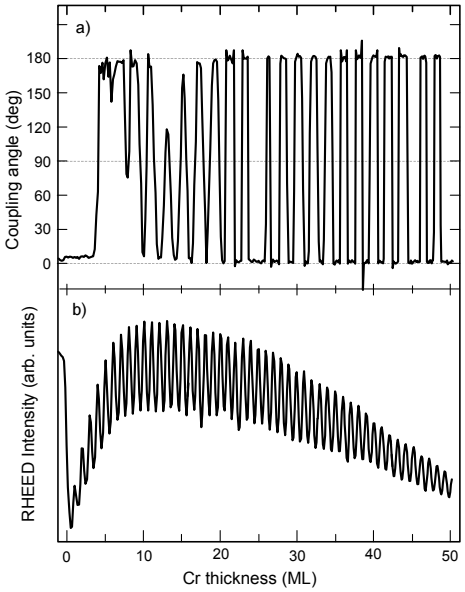
a)
b)
Coupling angle (deg)
180
150
120
90
60
30
0
RHEED Intensity (arb. units)
0
10
20
30
40
50
Cr thickness (ML)

Fig. 7